Design of Compact Reconfigurable Broadband Band-Stop Filter Based on a Low-Pass Filter Using Half Circle DGS Resonator and Multi-Layer Technique

Ahmed Boutejdar*

Abstract—This paper describes the design of a two-pole low-pass and band-stop filters. The low-pass structure is designed at the cutoff frequency of 2 GHz for the L-Band applications. This architecture uses half circle defected ground structure HCDGS instead full circle DGS resonator. Both the HCDGS shapes are etched in the ground plane and coupled via a substrate with a compensated capacitor. The rejection bandwidth of the LPF covers a large wideband spectrum. Therefore, the band suppression reaches more than $3fc$. The filter is simulated and fabricated. The measured results are in good agreement with the full-wave simulated ones, showing the merits of compact size and sharp roll-off. The multi-layer technique has been used in order to realize a transformation from low-pass behaviours to band-stop characteristics, keeping the same passband features. The new extracted band-stop topology is simulated and optimized using an RO4003 substrate with relative permittivity of 3.38 and thickness of $h = 0.813$ mm. The structure has a wide stopband with over 20 dB rejection from 3.5 GHz to 8.5 GHz. Such filters can be used for L-band and military applications.

1. INTRODUCTION

L-band low-pass filters (LPFs) have been used for satellite communications systems and radar systems [1–3]. The mobility of components and equipment is a requirement in mobile communication systems. Hence, great effort has gone into the compactness of devices. Further, various methods of wide banding have been devised for various functions. For this aim, different techniques have been proposed, such as cascaded resonators [4–6], step impedance resonators (SIRs) [7], microstrip ground structure (DMS) [8, 9] and defected ground structures (DGS) [10–16]. All of these techniques have some boundaries on the minimization of structure sizes, because they are based on half-wave resonators. Low-pass and band-stop filters have been studied and exploited extensively as a key in modern microwave areas and communication systems. Conventional microstrip filters are usually implemented using open stub or cascaded high-low impedance elements [17, 18]. To overcome these disadvantages, many researchers introduced designs of compact and uncomplicated microstrip filters employing photonic bandgap (PBG) [19] and defected ground structure (DGS) Fig. 1(a). Periodic or non-periodic defected ground structure (DGS) is realized by etching a slot in the backside metallic ground plane [20, 21]. Most DGS structures consist of two-dimensional periodic slot in the ground metallic plane. Several variations of area shapes such as triangle, square, circle, have different effects [22–24]. It is well known that in conventional DGS microstrip structures, there is always a tradeoff between the stopband and passband characteristics. Increasing the size of the etched slot would produce a wider stopband bandwidth and better stopband rejection at the expense of the passband. On the other hand, reducing the size of the slot would improve the return loss while degrading the stopband characteristics. In order to simultaneously

improve the passband and stopband performance of the DGS microstrip structures, some efforts have been reported in [10–12, 22]. However, the problem of DGS microstrip structure with good performance in both the passband and stopband was not fully solved.

In this paper, a new DGS low-pass microstrip filter using two electromagnetic coupled metal-loaded half-circle-head slots in the ground metallic plane is presented. The structure has a compact geometry, as shown in Fig. 1(b). The use of half-circle-head slots will be shown to give sharp cutoff frequency response as well as a good performance in both the passband and stopband. A circuit model has been developed to characterize the proposed low-pass filter. The model agrees with the field simulation results of Microwave Office [25] as shown in Fig. 1(c). The filter is simulated and fabricated. The results show good agreement between simulated and experimental data. The new extracted band-stop filter was designed and optimized using a patch octagonal resonator and multilayer technique. To improve the sharpness and thus stopband bandwidth, two symmetrical L-stepped impedance resonators are added at both sides of the octagonal patch capacitor. To show the tunability of this band-stop structure [26, 27], several variations of the microstrip capacitor-length are used.
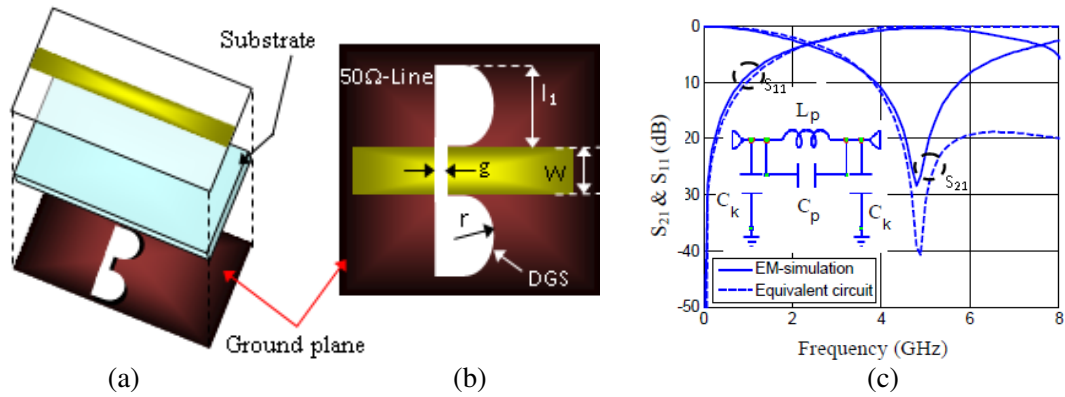
Figure 1. Layout of the half circle DGS resonator. (a) 3D-view, (b) 2D-view of the slot with its dimensions and (c) EM and equivalent circuit simulation results of the proposed half-circle-DGS.

2. CONFIGURATION AND EQUIVALENT CIRCUIT OF HALF-CIRCLE-DGS

The proposed DGS is symmetric and consists of two half-circles, which are connected to a rectangular slot, and all are etched on the bottom of the substrate as shown in Fig. 1. The rectangular slot corresponds to capacitor. The two half-circle heads correspond to inductance, and are connected together via a slot of 0.6 mm width as shown in Fig. 1(a). In many works, the conventional circuit parameters are extracted from an electromagnetic simulation by matching to a one-pole Butterworth band-stop filter response, as such in [10]. In this work, the extraction of the circuit will be realized through the field distribution method, shown in Fig. 1(b) and Fig. 2. The microstrip line on the top has a width of $w = 1.9$ mm, which guarantees a $50\,\Omega$ for characteristic impedance of the microstrip. The substrate relative permittivity and thickness are 3.38 and $h = 0.813$ mm, respectively. Dimensions shown in Fig. 1(b) are $g = 0.6$ mm, $r = l_1/2 = 2$ mm, and $w = 2$ mm. The DGS cell is simulated using Microwave Office. Simulation results are depicted in Fig. 1(c), which shows the characteristic of a one-pole low-pass filter. Thus we can get the attenuation pole frequency f_0 at 5.2 GHz and the 3-dB cutoff frequency f_c of the filter at 2.4 GHz. To confirm the validity of the presented equivalent model, the DGS unit has been designed and calculated. The circuit parameters for the derived equivalent circuit can be proved with the field's distribution method and can be extracted from the simulation result. The simulation result of the proposed DGS unit section can be matched to the one-pole Butterworth-type low-pass response, which has 3-dB cutoff frequency at 2.5 GHz and resonance frequency at 4.9 GHz as shown in Fig. 1(c). The proposed equivalent circuit shown in Fig. 2(b) can be easily calculated by using the prototype element value of the one-pole Butterworth response. The prototype element value is given by various references [11–13]. The parallel capacitance value for the given DGS unit dimension can be
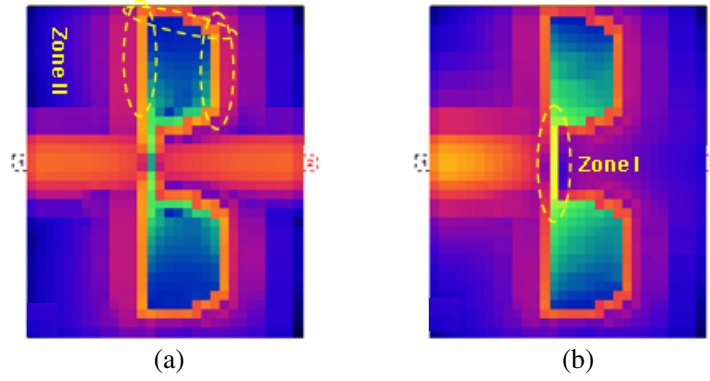
Figure 2. EM field distribution: (a) $f = 0.5\,\text{GHz}$, (b) $f = 5\,\text{GHz}$.

extracted from the attenuation pole location which exists at the resonance frequency of the parallel LC circuit- and prototype low-pass filter characteristics by using the following equations:

$$X_{LC} = \frac{\omega}{C_p \left(\omega_0^2 - \omega^2 \right)} \tag{1}$$

where ω_0, C_k and C_p are the resonance angular frequency of the parallel LC resonator, parasitic capacitor (negligible) and the capacitor of the DGS resonator, respectively. The schematic of one-pole Butterworth low-pass filter is shown in Fig. 2(b). The series inductance in the circuit can be written as:

$$X_L = \Omega Z_0 g_1 \tag{2}$$

In Eq. (2), Z_0 denotes the scaled impedance level of the in/out terminated ports, Ω the normalized angular frequency, and $g_1 = 2$ the normalized parameter of one-pole Butterworth lowpass filter that can be obtained from [11, 13, 19]. After the matching between the simulation result of the DGS unit section and the one-pole Butterworth-type low-pass response, the filter reactance values of both circuits are equal at the cutoff frequency. So L_p and C_p can be derived as follows:

$$X_{LC}\left.\right|_{\omega=\omega_c} = X_L\left.\right|_{\Omega=1} \tag{3}$$

$$\omega_0 = \frac{1}{\sqrt{C_p L_p}} \tag{4}$$

$$C_p = \frac{5 f_c}{\pi \left(f_0^2 - f_c^2 \right)}\,\text{pF} \quad \& \quad L_p = \frac{250}{C_p \left(\pi f_0 \right)}\,\text{nH} \tag{5}$$

3. EM-FIELD DISTRIBUTION ALONG OF THE PROPOSED DGS-RESONATOR

The surface electric and magnetic energies are introduced in order to observe the relationship between the EM-simulation results and the field distribution of the proposed DGS resonator as shown in Figs. 2(a), (b) [28]. The energy distribution is simulated at two different frequencies in the pass- and stop-bands. The first electromagnetic (EM) field distribution is at frequency 0.5 GHz and the second one at frequency 5 GHz. Around 0.5 GHz, almost the whole RF magnetic energy is transmitted from the input to the output and around the DGS (zone II), while a negligible electric energy appears in the gap (no metal), which signifies that the filter is in the passband state and that the metal area around the DGS has inductance behaviour as shown in Fig. 2(a). At 5 GHz, the flux-energy is blocked at the input of the structure. At the same time, the magnetic energy is distributed around the DGS while the electric energy is focused along the gap (between parallel metal strips) of DGS (zone I), which indicates that the structure is in the stopband state, and more precisely, the structure undergoes a resonance effect as Fig. 2(b) shows. Finally, it can be concluded that the full structure corresponds then to an LC-resonator. Briefly, this EM field distribution overcomes the limitation of reported full-wave analysis by developing the equivalent circuit model. This approach helps in understanding the physical principle

of DGS including how the DGS creates band-stop and bandpass responses and which dimensions play the most vital role to create the distinct performance.

The deviation at high frequency range between the EM simulation and circuit simulation appears because of the periodicity, while the electric signal of circuit cannot be periodic, and thus the response of the S_{21} remains flat along the high frequency range (Fig. 1(c)). Hence the two results agree well only along the low frequency range, more precisely between the DC and surroundings of the transmission zero, and only here the relationship remains valid.

4. DESIGN AND FABRICATION OF PROPOSED DGS-LPF

The DGS-filter is simulated on an RO4003 substrate with a relative permittivity of $\varepsilon_r = 3.38$ and thickness of $h = 0.813$ mm using an EM simulator, Microwave Office. Fig. 3 and Figs. 4(a), (b) show the layout of the proposed second order low-pass filter and the fabricated topology, respectively. Simulation results are compared with the measured ones as shown in Fig. 4(c).

The filter has 3-dB cutoff frequency fc at 3.8 GHz and an attenuation pole frequency f_0 at 5 GHz. However, as shown in Fig. 4(c), the suggested LPF which employs the half DGSs has lower loss in the passband and better rejection in the stopband than the conventional circle DGS LPF. This improvement
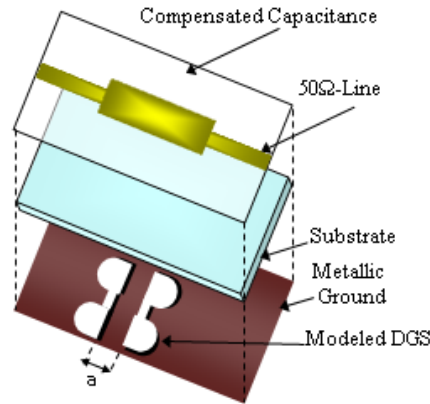
Figure 3. 3D-view of the proposed DGS-lowpass filter.
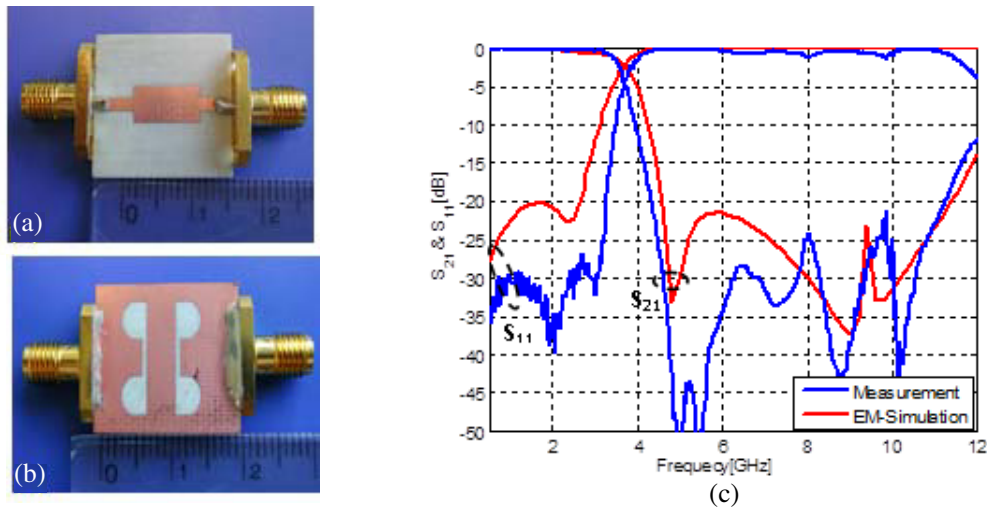
Figure 4. The photograph of the fabricated LPF: (a) Top view, (b) bottom view and (c) the comparison between simulation and measurement results of the DGS-LPF.

is due to the used slot's deformation, which leads to an increase of electric and magnetic coupling between the two neighbored DGS shapes. As shown in Fig. 3, the new slot geometry involves an additional electric and magnetic coupling, due to the gaps and slot heads, respectively. As presented in Fig. 4(c), a second transmission zero is regenerated and leads to an increase of the roll-off factor and to an extension of the reject band.

5. FABRICATION AND MEASUREMENT

A two-pole low-pass filter with half-circle-head DGSs has been fabricated on a substrate with dimensions of $30 \times 20 \, \text{mm}^2$. A substrate with a relative permittivity of 3.38 and thickness of 0.813 mm is used. Figs. 4(a), (b) show photographs of the fabricated half-circle DGS low-pass filter. Fig. 4(c) shows the comparison between the simulated and measured results by HP8719D network analyser, which agrees very well with the EM simulation results. It can be seen from the results that the fabricated HCDGS-LPF has an insertion loss less than 0.2 dB from DC to 3.7 GHz and selectivity (ξ) 17 dB/GHz. The attenuation characteristics show more than 20 dB from 4.2 GHz up to 11.3 GHz. Compared to conventional filters, the structure using half-DGS elements has wider and deeper stopband characteristic and sharper transition domain.

The selectivity of the filter can be extracted using the expressions given below:

$$Selectivity \, (\xi) = \frac{\alpha_{\min} - \alpha_{\max}}{f_s - f_c} \tag{6}$$

where $\alpha_{\min}$ and $\alpha_{\max}$ are the 20-dB and 3-dB attenuation, respectively, whereas f_s and f_c are the stop frequency at 20-dB attenuation and 3-dB cutoff frequencies. The unit of selectivity (ξ) is dB/GHz. A comparative study on the performances of the proposed half circle DGS LPF with various DGS filter-structures is shown in Table 1. According to results obtained and depicted in Table 1, the proposed filter topology delivers good LPF-features in stopband rejection and passband insertion loss and is smaller in size ($30 \times 20 \, \text{mm}^2$) than those reported in literature.

Table 1. Comparison of performance of proposed lowpass filter with various related LPF.

Reference filter	Selectivity (ξ) (dB/GHz)	Size (mm²)	fc (GHz)	S-B (GHz) (GHz) with $-20\,\text{dB}$	Pass-band I-L (dB)	Pass-band R-L (dB)
[5]	14.16	60×45	2.8	4–10	< 0.2	> 26
[10]	56.7	60×30	1.3	1.6–9	0.3	> 17
[1]	24.3	40×15	2.0	3–13	1	> 12
[18]	4.25	60×15	2.0	2.5–5.5	0.4	> 5
Proposed	17	30×20	3.7	4.2–11.3	0.2	> 27

6. THE BASIC IDEA OF LPF-BSF-TRANSITION

In order to convert the low-pass features to band-stop characteristics, a first grade multi-layer technique is employed. The used DGS shapes by LPF are moved to the top layer of the structure. As shown in Fig. 5(a), only one octagonal head will be used by the design of BSF topology. As shown in Fig. 5(b), the results of the band-stop filter are not satisfactory and do not meet required characteristics. Fig. 5(a) presents the layout view of the first proposed compact band-stop configuration. As depicted in Fig. 5(b), the band-stop behaviors appear. The dimensions of this topology shown in Fig. 5(b) are $l_1 = 20 \, \text{mm}$, $l_2 = 0.6 \, \text{mm}$, $w_0 = 1.9 \, \text{mm}$, $w_1 = 0.5 \, \text{mm}$, $r = 2 \, \text{mm}$, $d = 2 \, \text{mm}$ and $\theta = 45°$.

The structure shows a 20 dB stopband, which covers a frequency range of 1.5 GHz and a wide passband from DC to 3 GHz. The structure has a cutoff and a first reflexion zero at 3.5 GHz and 7.5 GHz, respectively. The topology is simulated on a similar substrate to before. The disadvantages of this filter are clearly seen in the transition domain and at stop region. As presented in Fig. 5(b), the transition curve nd reject band are not good enough. The presented sharpness is poor, and the bandwidth of stopband does not exceed 1.5 GHz.
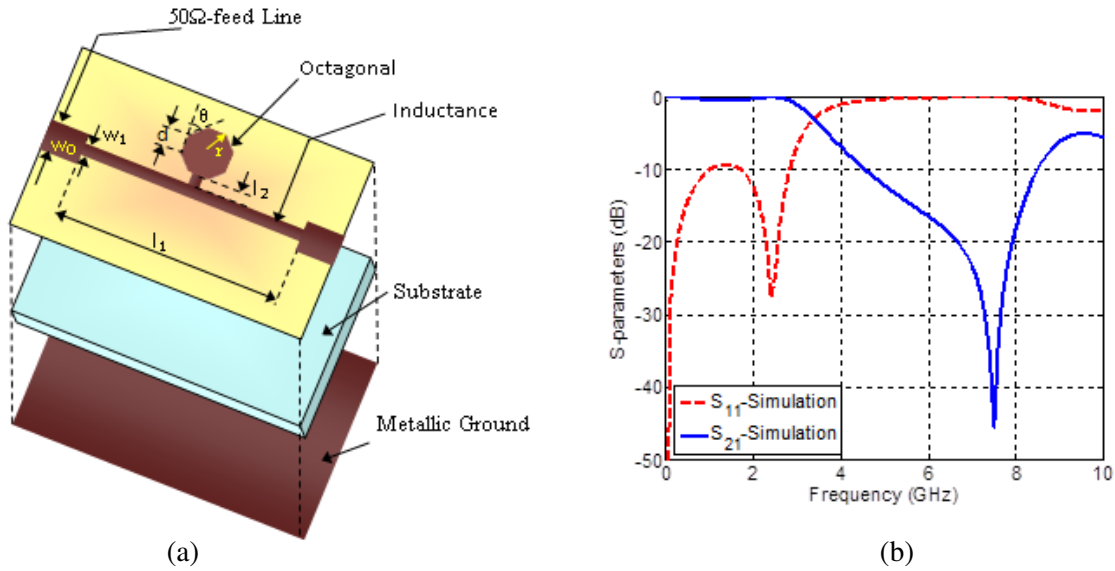
Figure 5. (a) Layout of the extracted BSF without DGS and without L-stepped impedance resonators, (b) the simulation results of extracted bandstop filter.

7. THE EXTRACTED BSF USING L-STEPPED IMPEDANCE RESONATOR

The goal of this research is focused on how to improve the reject band and minimize the loss of passband, while keeping the compact size as well as the other characteristics of the previous filter. For this aim, new symmetrically series resonators are at right and left of the octagonal patch capacitance (see Fig. 6(a)). The role of these added stepped impedances is to regenerate additional reflexion zeros of the stopband region and improve the transition domain. As shown in Fig. 6(b), the rejection band is extended over -20 dB from 3.5 GHz to 8.5 GHz. This stopband bandwidth is equal to $2fc$. Moreover, the size of the filter is $0.73\lambda_g \times 0.55\lambda_g$, in which $\lambda_g = 0.027$ m is the guided wavelength at the resonance frequency. The layout of the new improved compact band-stop topology is presented in Fig. 6(a). The dimensions of this resonator are defined using the empirical method, as follows: $l_5 = 5.5$ mm, $l_3 = 7.5$ mm, $l_4 = 4.5$ mm, $w_2 = 3.5$ mm.
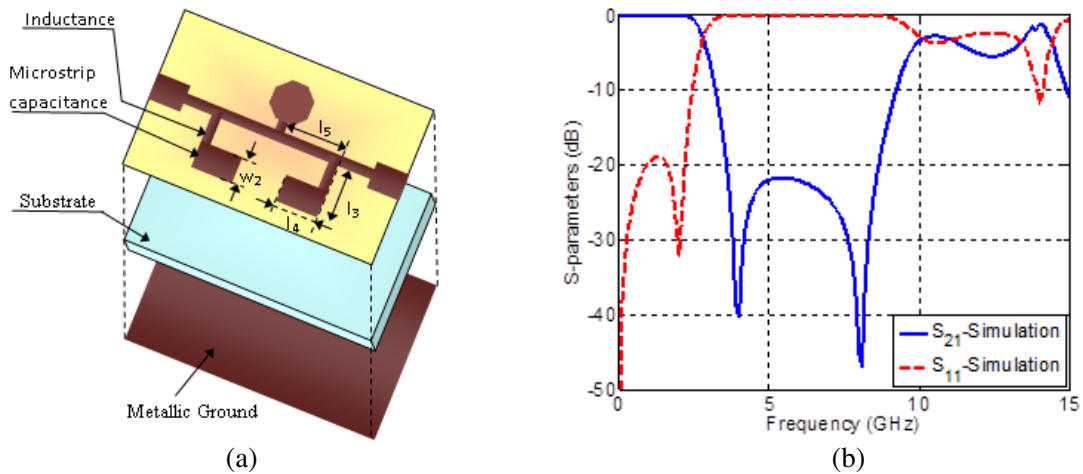
Figure 6. (a) Physical layout of proposed bandstop filter using two LCshaped stepped impedance resonators (LSSIRs), (b) its corresponding S-scattering results.

8. DISTRIBUTION OF MAGNETIC FIELD AT TRANSMISSION — AND REFLEXION ZERO

The purpose of this section is to show, based on the behaviours of surface magnetic energy, the relationship between the EM-simulation results and the field distribution of the proposed BSF. The field distribution is simulated at two different frequency poles, in the pass- and stop-bands. Around 1.5 GHz, almost the full RF magnetic energy is transmitted from the input to the output along the thin microstrip line (inductance). The resonator series are, because of high capacitance impedance, blocked, and thus the current is transmitted directly between the two ports of this structure, which signifies that the filter is in the passband, state and the metal strip has inductance behaviour as shown in Fig. 7(a). Fig. 7(b) shows the power distribution in the stopband region at the frequency of 3.8 GHz. At this frequency pole, the transmitted current is blocked at the input of the structure between input and the both first LC series resonators, which are connected in shunt across the main line. This means that the structure is in the stopband state, and more precisely, the structure undergoes a resonance effect as shown in Fig. 7.

(a)   (b)
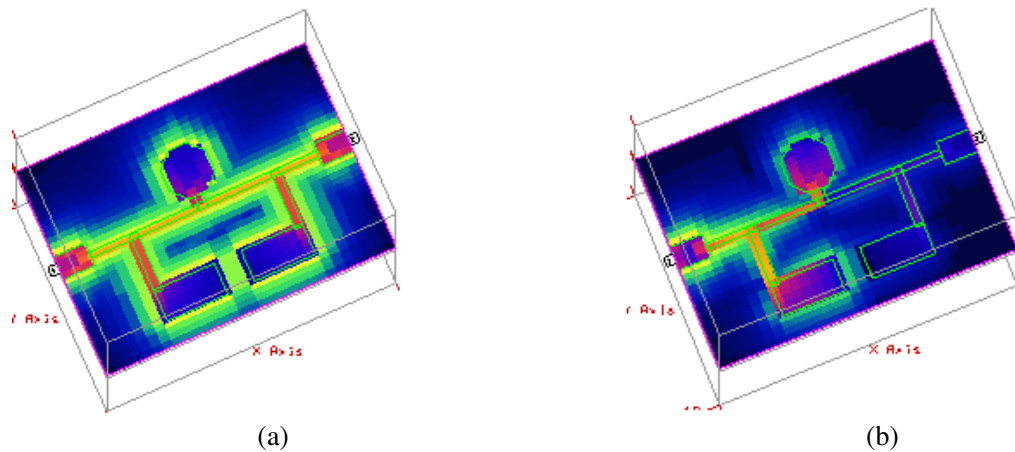
Figure 7. The field distribution at (a) 1.5 GHz, and at (b) 3.9 GHz of proposed new band-stop filter.

9. DESIGN OF IMPROVED COMPACT BAND-STOP FILTER USING VARIATION OF CAPACITANCE-LENGTH

In order to improve the compactness of the investigated filter without adding or withdrawing any part from the original structure, a length of the patch capacitor of the series resonator is increased. The increase of the length leads to increase of the capacitance values and per consequence a shift of the cutoff and resonance frequencies to low-frequency range, which means an increase of compactness of the structure. Fig. 8(a) shows a 3D-view of the proposed structure. As depicted in Fig. 8(b) and Fig. 6(b), the cutoff and resonance frequencies of the improved structure are 2.5 GHz and 3.8 GHz, respectively, while the two frequencies are 3 GHz and 4 GHz when the conventional structure is used. The new structure is simulated and optimized on the same RO4003 dielectric substrate using AWR electromagnetic simulator. The added L-stepped impedances play an interesting role in the improvement of compactness factor and control of the cutoff and position of attenuation pole without additional extra components.

10. DESIGN OF NEW TUNABLE BAND-STOP FILTER USING SYMMETRICAL L-STEPPED IMPEDANCE RESONATOR

To add tunability feature to this proposed filter, variable capacitors are placed as a bridge between the two patch capacitors of L-stepped resonators with the purpose to increase or decrease the total
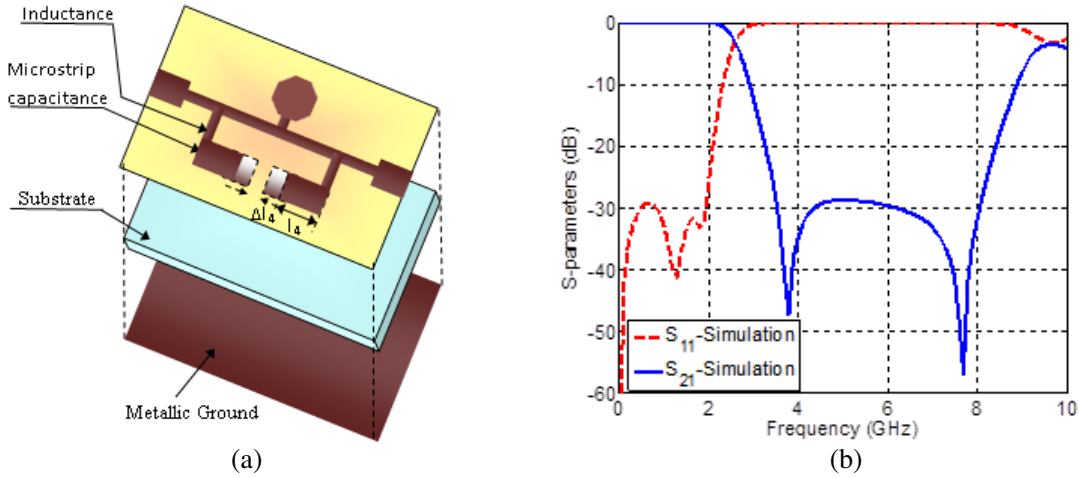
Figure 8. (a) Configuration and dimensions of improved BSF, (b) its simulation results.
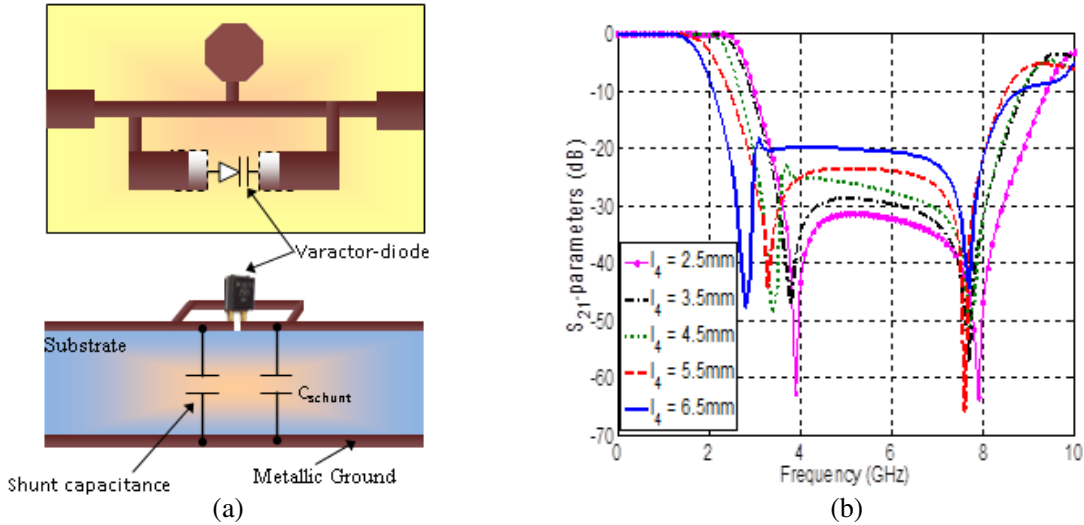
Figure 9. (a) layout of the new tunable band-stop filter using varactor-diode device. (upper): top view, (under): side view and (b) its corresponding simulated scattering S-parameter results.

capacitance value of the filter. Fig. 9(a) shows both top and side views of physical layout of the new tunable bandstop filter. As shown in Fig. 9(b), the variation of capacitor leads to a shift of the cutoff and attenuation pole in the low- or high-frequency ranges depending on capacitance values. In other words, the capacitance tuning allows a shift of the characteristics-frequencies to the low- or high-frequency domain depending on the used capacitance value. Using this technique, another method can be developed to obtain a flexible tunable filter [26, 27], which consists of a combination of passive microstrip components and active varactor-capacitor. Fig. 9(b) depicts different S-parameter results versus the length variation, which corresponds to the added capacitance. As depicted in Fig. 9(b), the cutoff frequency and attenuation pole move up to a lower frequency, while the value of the stub-length (varactor-capacitance) increases. The values of stub-length are varied from 2.5 mm to 6.5 mm while cutoff and first attenuation pole frequencies are varied from 2.7 GHz to 1.6 GHz and from 3.9 GHz to 2.8 GHz, respectively. To test our approach, the proposed band-stop filter is simulated and optimized to operate at 2.75 GHz. All filter dimensions and optimized scattering results are mentioned in Sections 6 and 7. The topology is designed, simulated and optimized on Rogers RO4003 substrates with relative permittivity of 3.38, thickness of 0.813 mm and loss tangent $\tan \delta = 0.0027$ using MWO simulator.

11. CONCLUSION

In this paper, a novel concept of a compact tunable band-stop filter using half-circle and L-stepped microstrip resonators is proposed. To design and realize this reconfigurable band-stop filter, we start with designing and manufacturing a low-pass filter using half-circle DGS resonator and compensating capacitor. The DGS low-pass filter consists of two cascaded DGS half-circle resonators and a compensated patch capacitor, placed on the top layer. Good pass- and stop-band performances as well as a minimized size are obtained. The new extracted band-stop filter is designed using a microstrip octagonal-head resonator and multilayer technique. To improve the roll-off factor and thus the stopband bandwidth, two symmetrical L-stepped resonators are added at the two sides of the middle circle patch resonator. To demonstrate the tunability of this band-stop topology, several variations of the length of capacitor are carried out. The reconfiguration characteristics can be shown in the future works by using a varactor capacitance. The measured frequency responses agree well with the simulation results, validating our proposed design. Such filter structures have the potential of being applied, because of their features, to RF/microwave integrated circuits.

REFERENCES

1. Yang, M., J. Xu, Q. Zhao, L. Peng, and G. Li, "Compact, broad-stopband lowpass filters using sirs-loaded circular hairpin resonators," *Progress In Electromagnetics Research*, Vol. 102, 95–106, 2010.

2. Liu, L., R. Jin, X. Bai, Y. Li, X. Liang, J. Geng, and C. He, "A tri-band bandstop filter with sharp rejection and controllable bandstop frequencies," *2015 IEEE International Symposium on Antennas and Propagation & USNC/URSI National Radio Science Meeting*, 2543–2544, 2015.

3. Yang, M., J. Xu, Q. Zhao, L. Peng, and G. Li, "Compact, broad-stopband lowpass filters using sirs-loaded circular hairpin resonators," *Progress In Electromagnetics Research*, Vol. 102, 95–106, 2010.

4. Boutejdar, A., G. Nadim, S. Amari, and A. S. Omar, "Control of bandstop response of cascaded microstrip low-pass-bandstop filters using arrowhead slots in backside metallic ground plane," *Proc. IEEE AP-Symp. (Washington DC)*, 2005.

5. Ahn, D., J. S. Park, C. S. Kim, J. Kim, Y. Qian, and T. Toh, "A design of the low-pass filter using the novel microstrip defected ground structure," *IEEE Trans. Microwave Theory Tech.*, Vol. 49, 86–93, 2001.

6. Nosrati, M., T. Faraji, and Z. Atlasbaf, "A compact composite broad stop-band elliptic function low-pass filter for ultra-wideband applications using interdigital capacitors," *Progress In Electromagnetics Research Letters*, Vol. 7, 87–95, 2009.

7. Wua, H.-W., C.-C. Lina, Y.-F. Chenb, and H.-Y. Leeb, "Compact triple-passband bandpass filter based on new modified stepped impedance resonators," *Microelectronics Journal*, Vol. 46, 490–495, 2015.

8. Boutejdar, A., A. Omar, and E. Burte, "High performance wide stop band low pass filter using a vertically coupled DGS-DMS-resonators and interdigital capacitor," *MOTL Microwave Opt. Technol. Lett.*, Vol. 56, 87–92, 2014.

9. Kazerooni, M., N. P. Gandji, A. Cheldavi, and M. Kamarei, "A new microwave bandstop filter using defected microstrip structure (DMS)," *PIERS Proceedings*, 697–700, Moscow, Russia, August 18–21, 2009.

10. Boutejdar, A., N. M. Eltabit, A. A. Ibrahim, and E. P. Burte, "Design of wide stop band L-band LPF based on DMS-DGS-technique for radar applications," *Hindawi Publishing Corporation International Journal of Microwave Science and Technology*, 7–13, Article ID 101602, 2015.

11. Hong, J. S., *Microstrip Filters for RF/Microwave Applications*, 2nd Edition, Wiley, New York, 2011.

12. Boutejdar, A., A. Elsherbini, and A. S. Omar, "A compact microstrip multi-layer lowpass filter using triangle slots etched in the ground plane," *Proc. 36th European Microwave Conference, 2006 (EuMC)*, Manchester, UK, September 2006.

13. Boutejdar, A., A. Abdel-Rahman, A. K. Verma, G. E. Nadim, and A. S. Omar, "Improved circuit model for DGS based lowpass filter," *Proc. IEEE AP-S Symp.*, 998–1001, Monterey, 2004.

14. Boutejdar, A., A. Elsherbini, S. Amari, M. Awida, and A. Omar, "Design of a novel microstrip bandstop filter using one compact C-open-loop resonator," *Asia-Pacific Microwave Conf., Yokohama*, Japan, December 2006.

15. Wang, C.-J. and T. H. Lin, "A multi-band meandered slotted-ground plane resonator and its application of low-pass filter," *Progress In Electromagnetics Research*, Vol. 120, 249–262, 2011.

16. Chen, J., Z.-B. Weng, Y.-C. Jiao, and F.-S. Zhang, "Lowpass filter design of hilbert curve ring defected ground structure," *Progress In Electromagnetics Research*, Vol. 70, 269–280, 2007.

17. Boutejdar, A., "A new approach to design compact tunable BPF starting from simple LPF topology using a single T-DGS-resonator and ceramic capacitors," *Microwave Opt. Technol. Lett.*, Vol. 58, 1142–1148, 2016.

18. Lu, K., G.-M. Wang, Y.-W. Wang, and X. Yin, "An improved design of Hi-Lo microstrip lowpass filter using uniplanar double spiral resonant cells," *Progress In Electromagnetics Research Letters*, Vol. 23, 89–98, 2011.

19. Chen, W.-L., G.-M. Wang, Y.-N. Qi, and J.-G. Liang, "Size-reduced fractal-shaped dual planar PBG microstrip low-pass filter," *7th International Symposium on Antennas, Propagation & EM Theory*, 1–4, 2006.

20. Boutejdar, A., W. Abd_Ellatif, A. A. Ibrahim, and M. Challal, "A simple transformation from lowpass to bandpass filter using a new quasi-arrow head defected ground structure resonator and gap-J-inverter," *Microwave Opt. Technol. Lett.*, Vol. 58, 947–953, 2016.

21. Boutejdar, A., "Entwurf, entwicklung und optimierung von kompakten HF-mikrostreifen-filtern mittels defected ground structure-technik (DGS)," doctorate degree (Dr. Eng.). At Otto-von-Guericke University, Magdeburg, November 2010.

22. Boutejdar, A., A. A. Ibrahim, and E. P. Burte, "Design of 5 GHz-compact reconfigurable dgs-bandpass filter using varactor-diode device and coupling matrix technique," *Microwave Opt. Technol. Lett.*, Vol. 58, 304–309, 2016.

23. Boutejdar, A., "Design of broad-stop band low pass filter using a novel quasi-Yagi-DGS-resonators and metal box-technique," *Microwave Opt. Technol. Lett.*, Vol. 56, 523–528, 2014.

24. Rahman, A. B., A. A. K. Verma, A. Boutejdar, and A. S Omar, "Control of bandstop response of Hi-Lo microstrip low-pass-filter using slot in ground plane," *IEEE Trans. Microwave Theory Tech.*, Vol. 52, 1008–1013, 2004.

25. AWR Microwave Office, Ver. 5.51, http://web.awrcorp.com.

26. Wu, Z., Y. Shim, and M. Rais-Zadeh, "Miniaturized UWB filters integrated with tunable notch filters using a silicon-based integrated passive device technology," *IEEE Trans. Microw. Theory and Tech.*, Vol. 60, 518–527, 2012.

27. Nosrati, M., N. Vahabisani, and M. Daneshmand, "Compact MEMS-based ultra wideband CPW band-pass filters with single/double tunable notch-bands," *IEEE Trans. Compon., Pack. Manufac Tech.*, Vol. 4, 1451–1460, 2014.

28. Boutejdar, A., et al., "Extracting of compact tunable BPF from LPF using single T-DGS-resonator and 0.25 PF/0.5 PF chip monolithic ceramic capacitors," *2015 4th International Conference on Electrical Engineering (ICEE)*, 1–5, Boumerdes, Algeria, 2015.